Engineering Analysis with Boundary Elements 33 (2009) 63–76

Contents lists available at ScienceDirect

Engineering Analysis with Boundary Elements

journal homepage: www.elsevier.com/locate/enganabound

A perturbation DRBEM model for weakly nonlinear wave run-ups around islands

Song-Ping Zhu [a,*], Huan-Wen Liu [b], Timothy R. Marchant [a]

[a] School of Mathematics and Applied Statistics, University of Wollongong, Wollongong, NSW 2522, Australia
[b] Department of Mathematics and Computer Science, Guangxi University for Nationalities, Nanning, Guangxi 530006, PR China

ARTICLE INFO

Article history:
Received 20 September 2007
Accepted 11 March 2008
Available online 16 June 2008

Keywords:
The dual reciprocity boundary element method (DRBEM)
Nonlinear Boussinesq equations
Wave diffraction and refraction

ABSTRACT

In this paper, the dual reciprocity boundary element method (DRBEM) based on the perturbation method is presented for calculating run-ups of weakly nonlinear long waves scattered by islands. Under the assumption that the incident waves are harmonic, the time-dependent nonlinear Boussinesq equations are transformed into three time-independent linear equations by using the perturbation method, where, besides nonlinearity ε, the dispersion μ^2 is also included in the perturbed expansion. The first-order solution η_0 is found by using the linear long-wave equations. Then η_0 is used in two second-order governing equations related to the dispersion and nonlinearity, respectively. Since no any omission and approximation for the seabed slope ∇h and its derivatives is made, there are the third- and fourth-order partial derivatives of η_0 appeared in the right-hand sides of two governing equations of the second-order. By employing a transformation, those third- and fourth-order partial derivatives are removed therefore large errors in approximating these derivatives are eliminated.

To validate the new model, wave diffractions around a large vertical cylinder for 13 cases are first considered. It is found that the nonlinear contributions to the new model are significant for weakly nonlinear waves with a much better comparison with experimental results obtained than for the linear diffraction theory. It is also found that the dispersive effects play an important role in improving the accuracy of the new model as numerical results obtained from the Boussinesq equations (with dispersion terms) are more accurate than those from the Airy's equations (without dispersion term). Then the combined wave diffraction and refraction by a conical island is also modelled and discussed. Our model is not only accurate as the dispersive effects have been included but also computationally efficient since the domain integrals are merely evaluated by distributing collocation points over that surface.

1. Introduction

Wave run-ups along the coast of islands are most significant during storm events such as hurricanes or cyclones. Due to the tremendous damage done during these events they have received significant attention in the past several decades. Because of the problem's complexity, the original three-dimensional governing equation is generally approximated by a two-dimensional version, such as the mild-slope equation and the Boussinesq equations. Despite these simplifications, only a few analytical models have been obtained, which are based on the Helmholtz equation [1], the linear long-wave equation [2–4] or the mild-slope equation [5]. Various numerical models have also been developed, which range from the numerical integration [6], the finite difference [7,8], hybrid finite elements [9–11], the orthogonal collocation [12], the conventional boundary elements [13] to the dual reciprocity boundary elements [14,15] or [16]. Islands studied with these models range from cylindrical islands [13], paraboloidal islands [11,12,14] to conical islands [6–8,15,17,18]. And the incident waves includes periodical plane waves [14,18] and solitary waves [7,8,18].

However, the range of water wave amplitudes that can be treated by most of these models is very restricted, being essentially limited to small-amplitude waves, described by linearized shallow-water wave equations, such as the Helmholtz equation, the linear shallow-water equation or the mild-slope equation. Although the results of these models based on linear governing equations may often provide some good approximation to the wave diffraction and refraction process, in reality, the experimental results suggest that the linearized theories give quite large errors in many practical situations. In fact, tsunamis are dramatically nonlinear in their final run-up stage.

* Corresponding author.
E-mail address: spz@uow.edu.au (S.-P. Zhu).

0955-7997/$ - see front matter Crown Copyright © 2008 Published by Elsevier Ltd. All rights reserved.
doi:10.1016/j.enganabound.2008.03.009

Based on various versions of the Boussinesq equations and the nonlinear shallow-water equations, some nonlinear numerical models have been developed. In terms of time integration, these models can be classified into two categories. Those in which the time integration is performed by step-by-step marching and those in which the explicit time integration has disappeared and problems are solved in a frequency domain.

In 1978, a time-marching finite-difference method based on the traditional Boussinesq equations [19] was developed by Abbott et al. [20]. In 1988, a line by line iterative method for the Boussinesq equations was proposed by Rygg [21]. Based on Nwogu's [22] improved Boussinesq equations, Wei and Kirby [23] developed a high-order numerical model where they used a fourth-order predictor-corrector scheme for time stepping and discretized the first-order spatial derivatives to fourth-order accuracy. Recently, based on the full-nonlinear Boussinesq equations [24], a time-domain numerical model was developed by Chen et al. [25] to simulate two laboratory experiments in large wave basins. In addition, based on the nonlinear shallow-water equation, a time-marching finite-difference method was proposed by Liu et al. [7,8], who studied the run-up of both solitary waves and periodic waves around a conical island and compared their numerical results with experimental results.

There is another way of solving nonlinear wave equations in the frequency-domain. Generally, we are interested in multiple frequencies, in which case all the sums and differences of frequency combinations need to be solved. From the point of view of computation, it is by no means obvious which approach is more efficient. Generally, to improve computing efficiency, we solve nonlinear wave equations in frequency-domain for a single main frequency or a few main frequencies. For example, Liu et al. [26] solved a parabolic approximation form of the traditional Boussinesq equations to the fifth harmonic. Chen and Liu [27] rederived the Nwogu's [22] modified Boussinesq equations in terms of a velocity potential on an arbitrary elevation and the free surface displacement, then solved two simplified forms in frequency-domain to the second-order harmonic.

In this paper, by using the assumption of harmonic waves and the perturbed expansion to the second order including a dispersive term, the time-dependent nonlinear Boussinesq equations are transformed into three time-independent linear systems, which are coupled by the water surface elevation and the depth-averaged horizontal velocity vector. Then these three coupled linear systems are decoupled and simplified into three linear equations. The first-order equation for η_0 is actually the linear long-wave equation. Since no any approximation for the seabed slope ∇h is used, there are third- and fourth-order partial derivatives of η_0 appeared in the right-hand sides of the two second-order equations. By employing a transformation, these third- and fourth-order partial derivatives of η_0 are successfully removed therefore large errors resulted from approximating these derivatives are eliminated. Up to this stage, the work left to us is to solve the three linear equations numerically.

The boundary element method (BEM) only requires a discretization on the boundary of a computational domain and it is popular to solve wave propagation problems with constant water depth (see [13,28]). However, when the water depth becomes a variable, the conventional BEM seems to be powerless because a domain integral arises; the evaluation of this domain integral in a traditional fashion through domain discretization destroys the elegance of the BEM, i.e., the dimension of the problem is reduced by one and only the boundary needs to be discretized.

To overcome this, employing the dual reciprocity boundary element method (DRBEM), which is originally developed by Nardini and Brebbia [29], Zhu [14] proposed a DRBEM wave model to solve the linear mild-slope equation. By comparing with hybrid finite elements [9–11], it was shown that the DRBEM model had a great advantage in numerical efficiency, in terms of both computational time and computer memory required. However, there was a restriction in Zhu's [14] DRBEM model as he had to make an assumption of a vertical-wall, i.e., the water depth being nonzero around the shoreline of the island. This assumption narrows down the range of application of the DRBEM model in comparison with its hybrid counterparts. Then Zhu et al. [15] (see also [16]) extended it to a general DRBEM (GDRBEM) model where cases with zero-water-depth coastlines can also be dealt with.

In this paper, the GDRBEM model is further extended to solve the three linear equations coming from the time-dependent nonlinear Boussinesq equations by using perturbation method. This leads to a new numerical model—the perturbation dual reciprocity boundary element method (PDRBEM). It must be pointed out that the acronym PDRBEM has already been used by Hsiao et al. [30,31] who combined the perturbation technique and the DRBEM, in order to improve the models proposed by Rangogni [32] and Zhu [14]. However, the governing equations used by Hsiao et al.'s [30,31] are different from the Boussinesq equation adopted as the governing equation in this paper.

In order to validate our new model, the wave run-ups around a large vertical cylinder for 13 different cases with weak nonlinearity are calculated and compared with experimental data [33,34], the linear diffraction theoretical solutions [1] and the second order diffraction theoretical solutions [33,34]. It is shown that both the nonlinear and dispersive contributions of the new model are significant for weakly nonlinear waves and that the new model provides a much better comparison with experimental results than the linear models. In addition, combined wave diffraction and refraction by a conical island are also tested for four cases. The run-ups from the PDRBEM are compared with experimental data [7], the linear theoretical solutions [3] and time-marching finite difference solutions which are based on the nonlinear shallow-water equation [7]. It is shown that the agreement among the PDRBEM solutions and experimental data and Liu et al.'s [7] solutions is overall satisfactory.

2. Governing equations

As illustrated in Fig. 1, we consider the weakly nonlinear refraction and diffraction of a plane monochromatic incident wave by an island standing on a seabed of otherwise constant water depth, h_0. Cartesian coordinates with the (x, y)-plane in the quiescent free surface and z positive upward are chosen. Since the monochromatic incident waves in the deep ocean can be regarded as linear waves, the corresponding potential can be

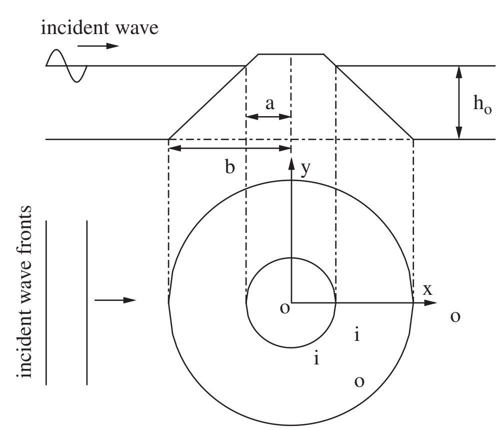

Fig. 1. A definition sketch: water waves scattered by a conical island.

expressed as

$$\zeta_{inc}(x,y,t)=\eta^I(x,y)e^{-i\omega t}=Ae^{i[k_0 r\cos(\theta-\theta^I)-\omega t]}$$
$$=A\sum_{n=0}^{\infty}\varepsilon_n i^n J_n(k_0 r)\cos n(\theta-\theta^I)e^{-i\omega t} \tag{1}$$

with A being the incident wave amplitude, ω the angular frequency, k_0 the wave number in constant-depth (h_0) water, θ^I the angle of incidence with respect to the x axis, and ε_n the Jacobi symbol ($\varepsilon_n=1$ for $n=0$ and $\varepsilon_n=2$ for $n>0$). The waves may be diffracted and reflected by the island and may also be refracted because of the change of water depth as they approach the island.

Let $\zeta(x,y,t)$ be the water surface elevation and $\mathbf{u}(x,y,t)=(u,v)$ the depth-averaged horizontal velocity vector. Introduce the following dimensionless quantities:

$$(x',y')=\frac{1}{\lambda}(x,y),\quad \zeta'=\frac{\zeta}{A},\quad t'=\frac{\sqrt{gh_0}}{\lambda}t,$$
$$h'=\frac{h}{h_0},\quad u'=\frac{h_0}{A\sqrt{gh_0}}u,\quad v'=\frac{h_0}{A\sqrt{gh_0}}v,\quad \omega'=\frac{\lambda}{\sqrt{gh_0}}\omega, \tag{2}$$

with λ being the wave length. For convenience the primes will be dropped from here now. If the scale of the water depth is small in comparison with the horizontal length scale and the wave amplitude is small compared with the water depth, i.e.

$$\mu^2=(h_0/\lambda)^2\ll 1,\quad \varepsilon=A/h_0\ll 1, \tag{3}$$

$\mathbf{u}$ and ζ may satisfy the so-called Boussinesq equations in dimensionless variables [19]

$$\begin{cases}\mathbf{u}_t+\nabla\zeta=-\varepsilon(\mathbf{u}\cdot\nabla)\mathbf{u}+\mu^2\dfrac{h}{2}\nabla[\nabla\cdot(h\mathbf{u}_t)]-\mu^2\dfrac{h^2}{6}\nabla(\nabla\cdot\mathbf{u}_t),\\ \zeta_t+\nabla\cdot(h\mathbf{u})=-\varepsilon\nabla\cdot(\zeta\mathbf{u}),\end{cases} \tag{4}$$

where two small parameters, ε and μ^2, are assumed to be of the same order. For very long waves: $\mu\to 0, \varepsilon=O(1)$, by omitting terms proportional to μ^2 from (4), we get the Airy equations [35, pp. 509–511].

If we assume that $\mathbf{u}$ and ζ are harmonic, they can be written as the following perturbation series:

$$\begin{cases}\mathbf{u}=(\mathbf{u}_0e^{-i\omega t}+\bar{\mathbf{u}}_0e^{i\omega t})+\mu^2(\mathbf{u}_1e^{-i\omega t}+\bar{\mathbf{u}}_1e^{i\omega t})\\ \quad +\varepsilon(\mathbf{u}_2e^{-i2\omega t}+\bar{\mathbf{u}}_2e^{i2\omega t}+\mathbf{u}_{2s}),\\ \zeta=(\eta_0e^{-i\omega t}+\bar{\eta}_0e^{i\omega t})+\mu^2(\eta_1e^{-i\omega t}+\bar{\eta}_1e^{i\omega t})\\ \quad +\varepsilon(\eta_2e^{-i2\omega t}+\bar{\eta}_2e^{i2\omega t}+\eta_{2s}),\end{cases} \tag{5}$$

where $\mathbf{u}_i=\mathbf{u}_i(x,y)$, $\eta_i=\eta_i(x,y)$, i = 0,1,2, and $\bar{\mathbf{u}}_i$ is the complex conjugate of $\mathbf{u}_i$. Then by substituting (5) into (4) and sorting out terms of the same order, the following three groups of equations are obtained

$$\begin{cases}-i\omega\mathbf{u}_0+\nabla\eta_0=0,\\ -i\omega\eta_0+\nabla\cdot(h\mathbf{u}_0)=0,\end{cases} \tag{6}$$

$$\begin{cases}-i\omega\mathbf{u}_1+\nabla\eta_1=-i\omega\dfrac{h}{2}\nabla[\nabla\cdot(h\mathbf{u}_0)]+i\omega\dfrac{h^2}{6}\nabla(\nabla\cdot\mathbf{u}_0),\\ -i\omega\eta_1+\nabla\cdot(h\mathbf{u}_1)=0,\end{cases} \tag{7}$$

$$\begin{cases}-i2\omega\mathbf{u}_2+\nabla\eta_2=-(\mathbf{u}_0\cdot\nabla)\mathbf{u}_0,\\ -i2\omega\eta_2+\nabla\cdot(h\mathbf{u}_2)=-\nabla\cdot(\eta_0\mathbf{u}_0),\end{cases} \tag{8}$$

$$\begin{cases}\nabla\eta_{2s}=-(\bar{\mathbf{u}}_0\cdot\nabla)\mathbf{u}_0-(\mathbf{u}_0\cdot\nabla)\bar{\mathbf{u}}_0,\\ \nabla\cdot(h\mathbf{u}_{2s})=-\nabla\cdot(\eta_0\bar{\mathbf{u}}_0+\bar{\eta}_0\mathbf{u}_0),\end{cases} \tag{9}$$

after $O(\varepsilon^2,\mu^4,\varepsilon\mu^2)$ terms are ignored. From (9), we can further have

$$\begin{cases}\eta_{2s}=-|\mathbf{u}_0|^2,\\ \mathbf{u}_{2s}=-\dfrac{1}{h}(\eta_0\bar{\mathbf{u}}_0+\bar{\eta}_0\mathbf{u}_0).\end{cases} \tag{10}$$

And the reflecting boundary condition along Γ_i is

$$h\bar{\mathbf{u}}\cdot\mathbf{n}=0, \tag{11}$$

which is equivalent to

$$h\bar{\mathbf{u}}_i\cdot\mathbf{n}=0,\quad i=0,1,2. \tag{12}$$

We now simplify Eqs. (6)–(8). Firstly, eliminating $\bar{\mathbf{u}}_0$ in (6), we can easily get the first-order governing equation

$$\nabla\cdot(h\nabla\eta_0)+\omega^2\eta_0=0, \tag{13}$$

which is the well-known linear long-wave equation. The corresponding boundary condition (12) along the coastline Γ_i is equivalent to

$$h\frac{\partial\eta_0}{\partial\mathbf{n}}=0. \tag{14}$$

In addition, a far-field radiation condition must be specified to ensure that the first-order scattered waves $\eta_0^s(x,y)$ behaves as outgoing waves propagating away from the island. Sommerfeld [36] gave the radiation condition as

$$\lim_{r\to\infty}\sqrt{r}\left(\frac{\partial\eta_0^s}{\partial r}-i\omega\eta_0^s\right)=0,\quad r=\sqrt{x^2+y^2}. \tag{15}$$

Secondly, eliminating $\bar{\mathbf{u}}_1$ in (7), we have

$$\begin{aligned}&\nabla\cdot(h\nabla\eta_1)+\omega^2\eta_1\\ &=i\omega\nabla\cdot\left[-\frac{h^2}{2}\nabla(\nabla\cdot(h\bar{\mathbf{u}}_0))+\frac{h^3}{6}\nabla(\nabla\cdot\bar{\mathbf{u}}_0)\right]\\ &=i\omega\nabla\cdot\left[-\frac{h^2}{2}\nabla(i\omega\eta_0)+\frac{h^3}{6}\nabla\left(\frac{1}{i\omega}\nabla^2\eta_0\right)\right]\\ &=\frac{\omega^2}{2}(2h\nabla h\cdot\nabla\eta_0+h^2\nabla^2\eta_0)+\frac{1}{6}[3h^2\nabla h\cdot\nabla(\nabla^2\eta_0)+h^3\nabla^2(\nabla^2\eta_0)]\\ &=\frac{\omega^2}{2}[2h\nabla h\cdot\nabla\eta_0+h(-\nabla h\cdot\nabla\eta_0-\omega^2\eta_0)]\\ &\quad+\frac{1}{6}[3h^2\nabla h\cdot\nabla(\nabla^2\eta_0)+h^3\nabla^2(\nabla^2\eta_0)]\\ &=-\frac{\omega^4}{2}h\eta_0+\frac{\omega^2}{2}h\nabla h\cdot\nabla\eta_0+\frac{h^2}{2}\nabla h\cdot\nabla(\nabla^2\eta_0)+\frac{h^3}{6}\nabla^2(\nabla^2\eta_0).\end{aligned} \tag{16}$$

This gives the second-order governing equation at the fundamental frequency

$$\begin{aligned}\nabla\cdot(h\nabla\eta_1)+\omega^2\eta_1=&-\frac{\omega^4h}{2}\eta_0+\frac{\omega^2h}{2}\nabla h\cdot\nabla\eta_0\\ &+\frac{h^2}{2}\nabla h\cdot\nabla(\nabla^2\eta_0)+\frac{h^3}{6}\nabla^2(\nabla^2\eta_0).\end{aligned} \tag{17}$$

Note that

$$\begin{aligned}h\frac{\partial\eta_1}{\partial\mathbf{n}}&=i\omega\left[h\bar{\mathbf{u}}_1-\frac{h^2}{2}\nabla(\nabla\cdot(h\bar{\mathbf{u}}_0))+\frac{h^3}{6}\nabla(\nabla\cdot\bar{\mathbf{u}}_0)\right]\cdot\mathbf{n}\\ &=i\omega\left[h\bar{\mathbf{u}}_1-\frac{h^2}{2}\nabla(i\omega\eta_0)+\frac{h^3}{6}\nabla\left(\frac{1}{i\omega}\nabla^2\eta_0\right)\right]\cdot\mathbf{n}\\ &=i\omega\left[h\bar{\mathbf{u}}_1-\frac{h^2}{2}i\omega\nabla\eta_0+\frac{h^3}{6}\frac{1}{i\omega}\nabla(\nabla^2\eta_0)\right]\cdot\mathbf{n}.\end{aligned}$$

The boundary condition (12) along the coastline Γ_i is equivalent to

$$h\frac{\partial\eta_1}{\partial\mathbf{n}}=\frac{h^3}{6}\frac{\partial(\nabla^2\eta_0)}{\partial\mathbf{n}}. \tag{18}$$

As to the far-field radiation condition for the scattered wave η_1, the Sommerfeld radiation condition can also be applied. But, since (17) is an inhomogeneous equation in an infinite region, we have to deal with a domain integral defined on the whole infinite region if the Sommerfeld radiation condition is applied to. In order to solve equation (17) numerically in a finite computational domain, an artificial boundary $\mathscr{B}$ must be set up and some sort of nonreflecting boundary condition along $\mathscr{B}$ need to be imposed. Since the 1970s, there have been many different nonreflecting boundary conditions proposed. A good review article was written by Givoli [37] on these conditions. As the Boussinesq equation is a weakly nonlinear long-wave equation with a small dispersive effect, we can choose a nonreflecting boundary condition for nondispersive waves proposed by Engquist and Majda [38]. Since the artificial boundary $\mathscr{B}$ in this paper is a circle and therefore the following nonreflecting boundary conditions in the polar coordinate system is used [37,38]

$$\frac{\partial\zeta}{\partial r}+\frac{\partial\zeta}{\partial t}+\frac{1}{2R}\zeta=0, \tag{19}$$

where R is the radius of the circle $\mathscr{B}$. In our case, this is simplified to

$$\frac{\partial\eta_1}{\partial\mathbf{n}}=\left(-\frac{1}{2R}+\mathrm{i}\omega\right)\eta_1. \tag{20}$$

Finally, eliminating $\bar{\mathbf{u}}_2$ in Eq. (8), we have the second-order governing equation for the nonlinear term η_2 involving the second-harmonic

$$\begin{aligned}\nabla\cdot(h\nabla\eta_2)+4\omega^2\eta_2 = {}& -2\nabla\eta_0\cdot\nabla\eta_0-2\eta_0\nabla^2\eta_0+\frac{1}{2\omega^2}\nabla h\cdot\nabla(\nabla\eta_0\cdot\nabla\eta_0)\\ &+\frac{1}{2\omega^2}h\nabla^2(\nabla\eta_0\cdot\nabla\eta_0).\end{aligned} \tag{21}$$

As the boundary condition (12) along the coastline Γ_i, we have

$$h\bar{\mathbf{u}}_2\cdot\mathbf{n}=0, \tag{22}$$

that is,

$$\begin{aligned}h\nabla\eta_2\cdot\mathbf{n}&=2\mathrm{i}\omega h\bar{\mathbf{u}}_2\cdot\mathbf{n}-h\nabla\left(\frac{1}{2}\bar{\mathbf{u}}_0\cdot\bar{\mathbf{u}}_0\right)\cdot\mathbf{n}\\ &=\frac{1}{2\omega^2}h\nabla(\nabla\eta_0\cdot\nabla\eta_0)\cdot\mathbf{n},\end{aligned}$$

which gives

$$h\frac{\partial\eta_2}{\partial\mathbf{n}}=\frac{h}{2\omega^2}\frac{\partial(\nabla\eta_0\cdot\nabla\eta_0)}{\partial\mathbf{n}}. \tag{23}$$

In addition, as to the far-field radiation condition for scattered wave η_2, as pointed by Kriebel [33, p. 353], a suitable far-field radiation condition for second-order scattered waves η_2 at the second-harmonic has not been completely well established though this problem has been extensively addressed by many researchers such as Molin [39], Kriebel [33] and Newman [40] when they attempted to give some second order perturbation solutions to the three-dimensional fully dispersive problem and various forms of the radiation conditions have been proposed. Among these radiation conditions the most commonly accepted one is proposed by Kriebel [33] in his second-order diffraction theory, which is a superposition of infinite localized Sommerfeld radiation conditions with respect to infinite source points. It is inconvenient to apply such kind of radiation condition in numerical calculation. Therefore in this paper, we still use Engquist and Majda's [38] nonreflecting boundary condition along the artificial boundary $\mathscr{B}$ for the second order scattered wave η_2. Similar to η_1, the corresponding nonreflecting condition for η_2 along $\mathscr{B}$ becomes

$$\frac{\partial\eta_2}{\partial\mathbf{n}}=\left(-\frac{1}{2R}+\mathrm{i}2\omega\right)\eta_2. \tag{24}$$

It is worth indicating that, both the second-order governing equation (17) for the fundamental frequency and (21) for the second-harmonic are inhomogeneous equations with their right-hand sides containing some partial derivatives of η_0 up to the fourth-order. All these derivatives will be approximated by using the first-order numerical solution η_0 and therefore large errors may result in representing these higher-order derivatives. Generally, the higher the order of the derivative is, the larger the error of the approximation is. In order to minimize these errors, we need to further simplify (17) and (21). In fact, we would not have been able to obtain a good result had the following transformation not been used. Introducing the transformation

$$\tilde{\eta}_1=\eta_1-\frac{h^2}{6}\nabla^2\eta_0, \tag{25}$$

we have from the governing equation (17)

$$\begin{aligned}&\nabla\cdot(h\nabla\tilde{\eta}_1)+\omega^2\tilde{\eta}_1\\ &\quad=-\frac{\omega^4}{2}h\eta_0+\frac{\omega^2}{2}h\nabla h\cdot\nabla\eta_0-\frac{\omega^2h^2}{6}\nabla^2\eta_0-\frac{1}{3}\nabla\cdot(h^2\nabla h\nabla^2\eta_0)\\ &\quad=-\frac{\omega^4}{2}h\eta_0+\frac{\omega^2}{2}h\nabla h\cdot\nabla\eta_0\\ &\qquad+\frac{\omega^2h}{6}(\nabla h\cdot\nabla\eta_0+\omega^2\eta_0)+\frac{1}{3}\nabla\cdot[h\nabla h(\nabla h\cdot\nabla\eta_0+\omega^2\eta_0)]\\ &\quad=-\frac{\omega^4h}{3}\eta_0+\frac{2\omega^2h}{3}\nabla h\cdot\nabla\eta_0+\frac{1}{3}\nabla\cdot(h\nabla h)(\nabla h\cdot\nabla\eta_0+\omega^2\eta_0)\\ &\qquad+\frac{h}{3}\nabla h\cdot\nabla(\nabla h\cdot\nabla\eta_0+\omega^2\eta_0)\\ &\quad=-\frac{\omega^2}{3}[\omega^2h-\nabla\cdot(h\nabla h)]\eta_0\\ &\qquad+\left[\omega^2h+\frac{1}{3}\nabla\cdot(h\nabla h)\right]\nabla h\cdot\nabla\eta_0+\frac{h}{3}\nabla h\cdot\nabla(\nabla h\cdot\nabla\eta_0).\end{aligned}$$

Hence, the second-order governing equation (17) is transformed into

$$\begin{aligned}\nabla\cdot(h\nabla\tilde{\eta}_1)+\omega^2\tilde{\eta}_1 = {}& -\frac{\omega^2}{3}[\omega^2h-\nabla\cdot(h\nabla h)]\eta_0\\ &+\left[\omega^2h+\frac{1}{3}\nabla\cdot(h\nabla h)\right]\nabla h\cdot\nabla\eta_0\\ &+\frac{h}{3}\nabla h\cdot\nabla(\nabla h\cdot\nabla\eta_0),\end{aligned} \tag{26}$$

which contains derivatives up to second-order only. The corresponding boundary conditions along Γ_i and the nonreflecting boundary conditions along $\mathscr{B}$ now become

$$h\frac{\partial\tilde{\eta}_1}{\partial\mathbf{n}}=\frac{h}{3}\frac{\partial h}{\partial\mathbf{n}}(\nabla h\cdot\nabla\eta_0+\omega^2\eta_0) \tag{27}$$

and

$$\frac{\partial\tilde{\eta}_1}{\partial\mathbf{n}}=\left(-\frac{1}{2R}+\mathrm{i}\omega\right)\tilde{\eta}_1+f_1(h,\eta_0), \tag{28}$$

with

$$\begin{aligned}f_1(h,\eta_0)={}&\frac{h}{6}\left(\frac{1}{2R}-\mathrm{i}\omega\right)(\nabla h\cdot\nabla\eta_0+\omega^2\eta_0)+\frac{\omega^2h}{6}\frac{\partial\eta_0}{\partial\mathbf{n}}\\ &+\frac{h}{6}\frac{\partial(\nabla h\cdot\nabla\eta_0)}{\partial\mathbf{n}}+\frac{1}{6}\frac{\partial h}{\partial\mathbf{n}}(\nabla h\cdot\nabla\eta_0+\omega^2\eta_0).\end{aligned} \tag{29}$$

Similarly, let

$$\tilde{\eta}_2=\eta_2-\frac{1}{2\omega^2}\nabla\eta_0\cdot\nabla\eta_0 \tag{30}$$

and the governing equation (21) for the second-harmonic now becomes

$$\nabla\cdot(h\nabla\tilde{\eta}_2)+4\omega^2\tilde{\eta}_2=-4\nabla\eta_0\cdot\nabla\eta_0-2\eta_0\nabla^2\eta_0. \tag{31}$$

The corresponding boundary conditions along Γ_i and the nonreflecting boundary conditions along $\mathscr{B}$, i.e., (23) and (24), respectively, become

$$h\frac{\partial\tilde{\eta}_2}{\partial\mathbf{n}}=0, \tag{32}$$

and

$$\frac{\partial \tilde{\eta}_2}{\partial \mathbf{n}} = \left(-\frac{1}{2R} + \mathrm{i}2\omega\right)\tilde{\eta}_2 + f_2(\eta_0), \tag{33}$$

with

$$f_2(\eta_0) = \frac{1}{2\omega^2}\left(-\frac{1}{2R} + \mathrm{i}2\omega\right)\nabla\eta_0 \cdot \nabla\eta_0 - \frac{1}{2\omega^2}\frac{\partial}{\partial \mathbf{n}}(\nabla\eta_0 \cdot \nabla\eta_0). \tag{34}$$

These three sets of differential systems are now solved with the DRBEM method.

3. Formation of integral equations

To solve (13), (26) and (31) together with their boundary conditions efficiently, we cast them into boundary integral equations. In this section, the integral equations corresponding too (13), (26) and (31) are given.

3.1. The first-order solution

The differential system (13) is defined on an infinite computational domain, which is usually divided into two sub-domains Ω_i and Ω_0 (see Fig. 1) with Ω_i denoting a finite inner domain with variable water depth and Ω_0 denoting an infinite outer domain in which no topographic variation is assumed so that only a constant water depth needs to be dealt with. The governing differential equations in these domains are of different forms and they will be discussed separately.

In domain Ω_i, Eq. (13) can be rewritten as

$$\nabla^2(h\eta_0) + \omega^2(h\eta_0) = R_0(x,y), \tag{35}$$

where

$$R_0(x,y) = \omega^2(h-1)\eta_0 + \nabla h \cdot \nabla\eta_0 + \eta_0\nabla^2 h. \tag{36}$$

Let

$$\eta^*(\xi,\mathbf{x}) = \frac{\mathrm{i}}{4}H_0^{(1)}(\omega\rho)$$

be the Hankel function of the first kind of zeroth order with $\rho = \|\xi - \mathbf{x}\|$ being the distance between a source point ξ and a field point $\mathbf{x} = (x,y)$. For any fixed source point ξ, multiplying both sides of Eq. (35) by $\eta^*(\xi,\mathbf{x})$ and using the Green's second identity, we can transform Eq. (35) into

$$c_\xi^{(i)}h(\boldsymbol{\xi})\eta_0(\boldsymbol{\xi}) + \int_{\Gamma_0+\Gamma_i}\left[h(\eta_0 q^* - q_0\eta^*) - \frac{\partial h}{\partial \mathbf{n}}\eta_0\eta^*\right]\mathrm{d}\Gamma = -\int_{\Omega_i} R_0\eta^*\,\mathrm{d}\Omega, \tag{37}$$

where $q^* = \partial\eta^*(\xi,\mathbf{x})/\partial\mathbf{n}$ and $q_0 = \partial\eta_0(\boldsymbol{\xi},\mathbf{x})/\partial\mathbf{n}$ with $\mathbf{n}$ being outward normal unit vector for the inner domain Ω_i, and $c_\xi^{(i)}$ is a geometric parameter which depends on the location of the source point ξ,

$$c_\xi^{(i)} = \begin{cases} \dfrac{\alpha(\boldsymbol{\xi})}{2\pi} & \text{if } \xi \in \Gamma_0 + \Gamma_i, \\ 1 & \text{if } \xi \in \Omega_i, \end{cases}$$

with $\alpha(\boldsymbol{\xi})$ being the internal angle of the boundary at point $\boldsymbol{\xi}$.

In the domain Ω_0, since the water depth is assumed to be constant, the free surface elevation η_0^s of the scattered wave should satisfy the Helmholtz equation

$$\nabla^2\eta_0^s + \omega^2\eta_0^s = 0. \tag{38}$$

Multiplying both sides of Eq. (38) by $\eta^*(\xi,\mathbf{x})$ and using Green's second identity and the Sommerfeld radiation condition (15) at infinity, we can transform Eq. (38) into

$$-c_\xi^{(o)}\eta_0^s(\xi) + \int_{\Gamma_0}\left(\frac{\partial\eta_0^s}{\partial\mathbf{n}'}\eta^* - \eta_0^s\frac{\partial\eta^*}{\partial\mathbf{n}'}\right)\mathrm{d}\Gamma = 0, \tag{39}$$

where $\mathbf{n}'$ is the outward normal unit vector of the outer domain Ω_0 and

$$c_\xi^{(o)} = \begin{cases} \dfrac{\alpha(\boldsymbol{\xi})}{2\pi} & \text{if } \xi \in \Gamma_0, \\ 0 & \text{if } \xi \in \Omega_i \cup \Gamma_i. \end{cases}$$

The continuity of the wave potential and flux across the common boundary Γ_0 shared by Ω_0 and Ω_i demands

$$\begin{cases} \eta_0 = \eta_0^s + \eta^I, \\ q_0 = -\left(\dfrac{\partial\eta_0^s}{\partial\mathbf{n}'} + \dfrac{\partial\eta^I}{\partial\mathbf{n}'}\right), \end{cases}$$

be satisfied on Γ_0. Therefore, Eq. (39) can be rewritten as

$$\int_{\Gamma_0}(\eta_0 q^* - q_0\eta^*)\,\mathrm{d}\Gamma = c_\xi^{(o)}\eta_0(\xi) - c_\xi^{(o)}\eta^I(\xi) + \int_{\Gamma_0}(\eta^I q^* - q^I\eta^*)\,\mathrm{d}\Gamma, \tag{40}$$

where $q^I = \partial\eta^I(\xi,\mathbf{x})/\partial\mathbf{n}$. Now, the two integral equations (37) and (40) can be merged into one

$$\begin{aligned} c_\xi h(\xi)\eta_0(\xi) &- \int_{\Gamma_0+\Gamma_i}\frac{\partial h}{\partial\mathbf{n}}\eta_0\eta^*\,\mathrm{d}\Gamma + h_i\int_{\Gamma_i}(\eta_0 q^* - q_0\eta^*)\,\mathrm{d}\Gamma \\ &= c_\xi^{(o)}h_0\eta^I(\xi) - h_0\int_{\Gamma_0}(\eta^I q^* - q^I\eta^*)\,\mathrm{d}\Gamma - \int_{\Omega_i}R_0\eta^*\,\mathrm{d}\Omega, \end{aligned} \tag{41}$$

where

$$c_\xi = \begin{cases} \dfrac{\alpha(\boldsymbol{\xi})}{2\pi} & \text{if } \xi \in \Gamma_i, \\ \dfrac{\alpha(\boldsymbol{\xi})}{\pi} & \text{if } \xi \in \Gamma_0, \\ 1 & \text{if } \xi \in \Omega_i. \end{cases}$$

After the boundary condition (14) is used, Eq. (41) becomes

$$\begin{aligned} c_\xi h(\xi)\eta_0(\xi) &- \int_{\Gamma_0+\Gamma_i}\frac{\partial h}{\partial\mathbf{n}}\eta_0\eta^*\,\mathrm{d}\Gamma + h_i\int_{\Gamma_i}\eta_0 q^*\,\mathrm{d}\Gamma \\ &= c_\xi^{(o)}h_0\eta^I(\xi) - h_0\int_{\Gamma_0}(\eta^I q^* - q^I\eta^*)\,\mathrm{d}\Gamma - \int_{\Omega_i}R_0\eta^*\,\mathrm{d}\Omega. \end{aligned} \tag{42}$$

3.2. The second-order fundamental frequency solution

Eq. (26) for the nonlinear contribution at the fundamental frequency is

$$\nabla^2(h\tilde{\eta}_1) + \omega^2(h\tilde{\eta}_1) = R_1(x,y), \tag{43}$$

where

$$\begin{aligned} R_1(x,y) = \omega^2(h-1)\tilde{\eta}_1 + \nabla h \cdot \nabla\tilde{\eta}_1 + \tilde{\eta}_1\nabla^2 h - \frac{\omega^2}{3}[\omega^2 h - \nabla\cdot(h\nabla h)]\eta_0 \\ + \left[\omega^2 h + \frac{1}{3}\nabla\cdot(h\nabla h)\right]\nabla h\cdot\nabla\eta_0 + \frac{h}{3}\nabla h\cdot\nabla(\nabla h\cdot\nabla\eta_0). \end{aligned}$$

Let $\Omega_{\mathscr{B}}$ be the domain between Γ_i and $\mathscr{B}$. Then Eq. (43) can be transformed into the following integral equation:

$$c_\xi^{(\mathscr{B})}h(\xi)\tilde{\eta}_1(\xi) - \int_{\Gamma_i+\mathscr{B}}\left(\frac{\partial(h\tilde{\eta}_1)}{\partial\mathbf{n}}\eta^* - h\tilde{\eta}_1 q^*\right)\mathrm{d}\Gamma = -\int_{\Omega_{\mathscr{B}}}R_1\eta^*\,\mathrm{d}\Omega, \tag{44}$$

where

$$c_\xi^{(\mathscr{B})} = \begin{cases} \dfrac{\alpha(\boldsymbol{\xi})}{2\pi} & \text{if } \xi \in \Gamma_i + \mathscr{B}, \\ 1 & \text{if } \xi \in \Omega_{\mathscr{B}}. \end{cases}$$

Using the nonreflecting condition on Γ_i and $\mathscr{B}$, we have

$$c_\xi^{(\mathscr{B})} h(\xi)\tilde{\eta}_1(\xi) - \int_{\Gamma_i+\mathscr{B}} \left[\frac{\partial h}{\partial \mathbf{n}}\tilde{\eta}_1\eta^* - h\tilde{\eta}_1 q^*\right] d\Gamma + \int_{\mathscr{B}} h\left(\frac{1}{2R} - i\omega\right)\tilde{\eta}_1\eta^* \, d\Gamma - \int_{\Gamma_i} \frac{h}{3}\frac{\partial h}{\partial \mathbf{n}}(\nabla h \cdot \nabla \eta_0 + \omega^2 \eta_0)\eta^* \, d\Gamma - \int_{\mathscr{B}} h f_1(h, \eta_0)\eta^* \, d\Gamma = -\int_{\Omega_{\mathscr{B}}} R_1 \eta^* \, d\Omega. \tag{45}$$

3.3. The second-order solution for the second-harmonic

The governing equation (31) for the second-harmonic can be rewritten as

$$\nabla^2(h\tilde{\eta}_2) + 4\omega^2(h\tilde{\eta}_2) = R_2(x,y), \tag{46}$$

where

$$R_2(x,y) = 4\omega^2(h-1)\tilde{\eta}_2 + \nabla h \cdot \nabla \tilde{\eta}_2 + \tilde{\eta}_2 \nabla^2 h - 4\nabla\eta_0 \cdot \nabla\eta_0 - 2\eta_0\nabla^2\eta_0.$$

Let

$$\eta_2^*(\xi, \mathbf{x}) = \frac{i}{4} H_0^{(1)}(2\omega\rho).$$

Multiplying both sides of Eq. (46) by η_2^* and using the Green's second identity, we can transform Eq. (46) into

$$c_\xi^{(\mathscr{B})} h(\xi)\tilde{\eta}_2(\xi) - \int_{\Gamma_i+\mathscr{B}} \left[\frac{\partial(h\tilde{\eta}_2)}{\partial \mathbf{n}}\eta_2^* - h\tilde{\eta}_2 q_2^*\right] d\Gamma = -\int_{\Omega_{\mathscr{B}}} R_2\eta_2^* \, d\Omega, \tag{47}$$

where $q_2^* = \partial\eta_2^*(\xi, \mathbf{x})/\partial\mathbf{n}$. Using the boundary condition on Γ_i and the nonreflecting boundary condition on $\mathscr{B}$, we have

$$c_\xi^{(\mathscr{B})} h(\xi)\tilde{\eta}_2(\xi) - \int_{\Gamma_i+\mathscr{B}} \left[\frac{\partial h}{\partial \mathbf{n}}\tilde{\eta}_2\eta_2^* - h\tilde{\eta}_2 q_2^*\right] d\Gamma + \int_{\mathscr{B}} h\left(\frac{1}{2R} - i2\omega\right)\tilde{\eta}_2\eta_2^* \, d\Gamma - \int_{\mathscr{B}} h f_2(\eta_0)\eta_2^* \, d\Gamma = -\int_{\Omega_{\mathscr{B}}} R_2\eta_2^* \, d\Omega. \tag{48}$$

4. The dual reciprocity boundary elements

The DRBEM was first proposed by Nardini and Brebbia [29] and later improved by many others, for example, Nardini and Brebbia [41], Partridge and Wrobel [42], Zhu and Zhang [43] and Zhang and Zhu [44]. Based on these theoretical results and the mild-slope equation, Zhu [14] first proposed a DRBEM wave model for wave diffraction and refraction on a paraboloidal island with a vertical-wall assumption around the coastline. Zhu et al. [15] further extended it to a general DRBEM (GDRBEM) model which can also work for a conical island without the vertical-wall assumption. For the completeness of the current paper, we shall also briefly describe the DRBEM here.

Firstly, the function $R_p(x,y)$, $p = 0,1,2$, in Eqs. (42), (45) and (48) are expanded as a series of radial basis functions (RBF) $f_j(\mathbf{x})$, i.e.:

$$R_p(\mathbf{x}) \approx \sum_{j=1}^{n+m+l} \alpha_j^{(p)} f_j(\mathbf{x}), \quad p = 0,1,2, \tag{49}$$

where $\alpha_j^{(p)}$ are the coefficients to be determined with the collocation method by demanding the satisfaction of $m+n+l$ equations

$$R_p(\mathbf{x}_i) = \sum_{j=1}^{n+m+l} \alpha_j^{(p)} f_j(\mathbf{x}_i), \quad i = 1, \ldots, n+m+l, \tag{50}$$

at n points on the boundary Γ_i, m points on Γ_0 (or $\mathscr{B}$) and l interior collocation points within the domain Ω_i (or $\Omega_{\mathscr{B}}$).

There are many different forms of RBF one may choose, ranging from the polynomial form shown in Partridge and Brebbia [45] to more exotic ones such as TPS (thin plate splines, cf. [46]), ATPS (augmented thin plate splines, [47]), MQ (multiquadric bases, cf. [48]), imaginary-part of the fundamental solution of the Helmholtz operator (cf. [49]), imaginary-part of the fundamental solution of the bi-harmonic operator (cf. [50]) and Chebyshev polynomials (cf. [51]). In terms of the choice of RBF, various researchers seem to have drawn, sometimes, totally different conclusions (cf. [52]). In this paper, we adopted

$$f_j(\mathbf{x}) = 1 + \|\mathbf{x} - \mathbf{x}_j\|^2 + \|\mathbf{x} - \mathbf{x}_j\|^3, \quad j = 1, \ldots, n+m+l.$$

as our radial basis functions for its simplicity. This particular form was recommended by Zhang and Zhu [44], after they had performed a number of numerical tests and comparisons with some other forms of RBFs. More recently, Hsiao et al. [52] gave a comprehensive review of the choice of RBF and conducted a series of numerical experiments, comparing TPS and a special form of polynomials and concluded that TPS has demonstrated significant improvement in accuracy. Our own numerical experience, on the other hands, showed that the adopted RBF had delivered satisfactory results and we have thus decided to adopt the form shown above.

System (50) can also be expressed in matrix form:

$$\mathbf{R}_p = \mathbf{F}\alpha^{(p)}, \quad p = 0,1,2, \tag{51}$$

in which the matrix $\mathbf{F}$, by Micchelli's theorem [53], is invertible. Therefore, we can express $\boldsymbol{\alpha}^{(p)}$ in terms of $\mathbf{F}^{-1}$ and $\mathbf{R}_p$ as

$$\boldsymbol{\alpha}^{(p)} = \mathbf{F}^{-1}\mathbf{R}_p, \quad p = 0,1,2. \tag{52}$$

The conversion of the domain integrals in Eqs. (42), (45) and (48) hinges on whether or not particular solutions $\hat{\eta}_j^{(p)}$, $p = 0,1,2$, can be found so that

$$\nabla^2\hat{\eta}_j^{(p)} + \omega_p^2\hat{\eta}_j^{(p)} = f_j(x,y), \tag{53}$$

for a given function f_j, where $\omega_0 = \omega_1 = \omega$ and $\omega_2 = 2\omega$. The existence and the recursion formulae for such kind of solutions have been found by Zhu [54]. Therefore, the domain integrals in Eqs. (42), (45) and (48) can be transformed into boundary integrals along boundaries:

$$\int_{\mathscr{D}} R_p(x,y)\eta^* \, d\Omega \approx \sum_{j=1}^{n+m+l} \alpha_j^{(p)} \left[-c_\xi^{(i)}\hat{\eta}_j^{(p)}(\xi) + \int_\Gamma (\hat{q}_j^{(p)}\eta^* - \hat{\eta}_j^{(p)}q^*) \, d\Gamma\right], \quad p = 0,1,2,$$

where $\mathscr{D}$ represents Ω_i or $\Omega_{\mathscr{B}}$ and Γ represents $\Gamma_i + \Gamma_0$ or $\Gamma_i + \mathscr{B}$, and $\hat{q}_j^{(p)} = \partial\hat{\eta}_j^{(p)}/\partial\mathbf{n}$. Consequently Eqs. (42), (45) and (48) can be rewritten as

$$c_\xi h\eta_0 - \int_{\Gamma_0+\Gamma_i} \frac{\partial h}{\partial \mathbf{n}}\eta_0\eta^* \, d\Gamma + h_i \int_{\Gamma_i} \eta_0 q^* \, d\Gamma = h_0 c_\xi^{(o)}\eta^I - h_0 \int_{\Gamma_0} (\eta^I q^* - q^I\eta^*) \, d\Gamma + \sum_{j=1}^{n+m+l} \alpha_j^{(0)} \left[c_\xi^{(i)}\hat{\eta}_j^{(0)} - \int_{\Gamma_0+\Gamma_i} (\hat{q}_j^{(0)}\eta^* - \hat{\eta}_j^{(0)}q^*) \, d\Gamma\right], \tag{54}$$

$$c_\xi^{(\mathscr{B})} h\tilde{\eta}_1 - \int_{\Gamma_i+\mathscr{B}} \left[\frac{\partial h}{\partial \mathbf{n}}\tilde{\eta}_1\eta^* - h\tilde{\eta}_1 q^*\right] \mathrm{d}\Gamma + \int_{\mathscr{B}} h\left(\frac{1}{2R} - \mathrm{i}\omega\right)\tilde{\eta}_1\eta^* \,\mathrm{d}\Gamma$$
$$- \int_{\Gamma_i} \frac{h}{3}\frac{\partial h}{\partial \mathbf{n}}(\nabla h\cdot\nabla\eta_0 + \omega^2\eta_0)\eta^*\,\mathrm{d}\Gamma - \int_{\mathscr{B}} hf_1(h,\eta_0)\eta^*\,\mathrm{d}\Gamma$$
$$= \sum_{j=1}^{n+m+l} \alpha_j^{(1)}\left[c_\xi^{(\mathscr{B})}\hat{\eta}_j^{(1)} - \int_{\Gamma_i+\mathscr{B}} (\hat{q}_j^{(1)}\eta^* - \hat{\eta}_j^{(1)} q^*)\,\mathrm{d}\Gamma\right], \tag{55}$$

$$c_\xi^{(\mathscr{B})} h\tilde{\eta}_2 - \int_{\Gamma_i+\mathscr{B}} \left[\frac{\partial h}{\partial \mathbf{n}}\tilde{\eta}_2\eta_2^* - h\tilde{\eta}_2 q_2^*\right] \mathrm{d}\Gamma$$
$$+ \int_{\mathscr{B}} h\left(\frac{1}{2R} - \mathrm{i}2\omega\right)\tilde{\eta}_2\eta_2^*\,\mathrm{d}\Gamma - \int_{\mathscr{B}} hf_2(\eta_0)\eta_2^*\,\mathrm{d}\Gamma$$
$$= \sum_{j=1}^{n+m+l} \alpha_j^{(2)}\left[c_\xi^{(\mathscr{B})}\hat{\eta}_j^{(2)} - \int_{\Gamma_i+\mathscr{B}} (\hat{q}_j^{(2)}\eta_2^* - \hat{\eta}_j^{(2)} q_2^*)\,\mathrm{d}\Gamma\right]. \tag{56}$$

Eqs. (54)–(56), involve boundary integrals only, after appropriate discretization and approximation to all derivatives of η_0, $\tilde{\eta}_1$ and $\tilde{\eta}_2$, a linear system of algebraic equations involving the unknown function η_0 on $\Gamma_i+\Gamma_0+\Omega_i$ or $\tilde{\eta}_1$ and $\tilde{\eta}_2$ on $\Gamma_i+\mathscr{B}+\Omega_{\mathscr{B}}$ can be established. The details of such a system is similar to those in Appendix A in Zhu et al. [15].

It should also be mentioned, in passing, that another mesh-free technique that has been developed after the DRBEM is the so-called MFS-DRM approach. While the MFS stands for the method of fundamental solutions (cf. [55]), the concept of the MPS, which stands for the method of particular solutions (also called method of particular integral), is used so that the advantage of MPS is taken while the inherent difficulty associated with this approach of finding a particular solution of the inhomogeneous differential operator can be avoided. This is achieved with a particular solution being represented by the radial-basis-function expansion adopted in DRM. Since the details of these approaches are beyond the scope of this paper, interested readers are referred to Li et al. [56].

5. Run-ups of nonlinear waves

After η_0, η_1 and η_2 are solved numerically, the next step is to calculate the maximum wave run-up. For the linear case this is very simple. In fact, let

$$\zeta(x,y,t) = \eta_0(x,y)\mathrm{e}^{-\mathrm{i}\omega t} = a_0\mathrm{e}^{-\mathrm{i}\omega t} + \mathrm{i}b_0\mathrm{e}^{-\mathrm{i}\omega t}$$
$$= (a_0\cos\omega t + b_0\sin\omega t) + \mathrm{i}(b_0\cos\omega t - a_0\sin\omega t),$$

where a_0 and b_0 are the real and imaginary parts of η_0, respectively. The surface elevation $\zeta_{phys}(x,y,t)$ is the real part of ζ and the run-up is given by the maximum value of $\zeta_{phys}(x,y,t)$. This is

$$\max_t \zeta_{phys}(x,y,t) = \max_t\left(\sqrt{a_0^2+b_0^2}\sin(\omega t+\theta_0)\right)$$
$$= \sqrt{a_0^2+b_0^2}, \tag{57}$$

where

$$\theta_0 = \begin{cases} \tan^{-1}\dfrac{a_0}{b_0} & \text{if } b_0>0,\\ \dfrac{\pi}{2}+\tan^{-1}\dfrac{a_0}{b_0} & \text{if } b_0<0,\\ \dfrac{\pi}{2} & \text{if } b_0=0,\ \ a_0>0,\\ -\dfrac{\pi}{2} & \text{if } b_0=0,\ \ a_0<0. \end{cases}$$

Also, we have

$$\max_t|\zeta(x,y,t)|$$
$$= \max_t\sqrt{(a_0\cos\omega t+b_0\sin\omega t)^2+(b_0\cos\omega t-a_0\sin\omega t)^2}$$
$$= \sqrt{a_0^2+b_0^2}.$$

This means, for linear waves, we have

$$\max_t \zeta_{phys}(x,y,t) = \max_t|\zeta(x,y,t)|. \tag{58}$$

For weakly nonlinear waves, according to expression (5), the total (complex) instantaneous surface elevation is

$$\zeta(x,y,t) = \eta_0(x,y)\mathrm{e}^{-\mathrm{i}\omega t} + \mu^2\eta_1(x,y)\mathrm{e}^{-\mathrm{i}\omega t} + \varepsilon\eta_2(x,y)\mathrm{e}^{-\mathrm{i}2\omega t}$$
$$= (a_{01}(x,y)+\mathrm{i}b_{01}(x,y))\mathrm{e}^{-\mathrm{i}\omega t} + (a_2(x,y)+\mathrm{i}b_2(x,y))\mathrm{e}^{-\mathrm{i}2\omega t}$$
$$= (a_{01}\cos\omega t+b_{01}\sin\omega t) + \mathrm{i}(b_{01}\cos\omega t - a_{01}\sin\omega t)$$
$$+ (a_2\cos2\omega t+b_2\sin2\omega t) + \mathrm{i}(b_2\cos2\omega t - a_2\sin2\omega t).$$

And the physical surface elevation is the real part of this expression, that is,

$$\zeta_{phys}(x,y,t) = a_{01}\cos\omega t + b_{01}\sin\omega t + a_2\cos2\omega t + b_2\sin2\omega t$$
$$= \sqrt{a_{01}^2+b_{01}^2}\sin(\omega t+\theta_1) + \sqrt{a_2^2+b_2^2}\sin(2\omega t+\theta_2), \tag{59}$$

where

$$\theta_1 = \begin{cases} \tan^{-1}\dfrac{a_{01}}{b_{01}} & \text{if } b_{01}>0,\\ \dfrac{\pi}{2}+\tan^{-1}\dfrac{a_{01}}{b_{01}} & \text{if } b_{01}<0,\\ \dfrac{\pi}{2} & \text{if } b_{01}=0,\ \ a_{01}>0,\\ -\dfrac{\pi}{2} & \text{if } b_{01}=0,\ \ a_{01}<0 \end{cases}$$

and

$$\theta_2 = \begin{cases} \tan^{-1}\dfrac{a_2}{b_2} & \text{if } b_2>0,\\ \dfrac{\pi}{2}+\tan^{-1}\dfrac{a_2}{b_2} & \text{if } b_2<0,\\ \dfrac{\pi}{2} & \text{if } b_2=0,\ \ a_2>0,\\ -\dfrac{\pi}{2} & \text{if } b_2=0,\ \ a_2<0. \end{cases}$$

Also in contrast to the linear case, relationship (58) does not hold for the nonlinear case. In fact, since

$$|\zeta(x,y,t)|^2 = a_{01}^2+b_{01}^2+a_2^2+b_2^2+2(a_{01}a_2+b_{01}b_2)\cos\omega t$$
$$+2(a_{01}b_2-b_{01}a_2)\sin\omega t, \tag{60}$$

we have

$$\max_t|\zeta(x,y,t)| = \sqrt{a_{01}^2+b_{01}^2}+\sqrt{a_2^2+b_2^2}, \tag{61}$$

so by comparison with (58) it can be seen that is not true in the nonlinear case. Thus, to obtain run-ups of the nonlinear waves in this paper, we need to calculate the maximum value

$$\max_t\left(\sqrt{a_{01}^2+b_{01}^2}\sin(\omega t+\theta_1)+\sqrt{a_2^2+b_2^2}\sin(2\omega t+\theta_2)\right).$$

Note that, the periods of $\sin(\omega t+\theta_1)$ and $\sin(2\omega t+\theta_2)$ are $2\pi/\omega$ and π/ω, respectively, the period of $\zeta_{phys}(x,y,t)$ is $2\pi/\omega$ and the maximum value of $\zeta_{phys}(x,y,t)$ must appear in the interval $[0,2\pi/\omega]$. Hence, numerically, we can easily find out the maximum value in the period $[0,2\pi/\omega]$.

6. Numerical examples

To test the PDRBEM model, we calculated wave amplification around coastlines for both a vertical cylinder and a circular conical island and compare our results with experimental data, linear theoretical solutions and other numerical solutions. For simplicity, the incident angle θ^I of the incident waves is taken to be 0° and all the variables are now referred back to dimensional quantities.

6.1. Diffraction around a vertical cylinder

For wave diffraction on a vertical cylinder, there have been many experiments conducted for various kinds of cylinders and incident waves. However most of them only concerned wave forces rather than wave run-ups. Data from wave run-up experiments are somewhat limited, only found in a few literature, the cylinders studied in those literature are usually small and the waves are usually linear waves with very small amplitudes anyway.

Recently, Kriebel [33,34] developed a nonlinear diffraction theory for wave–structure interaction to the second order where a set of experimental data of nonlinear wave run-ups was presented and compared with his second-order diffraction theoretical solutions. According to Kriebel [33,34], a total of 22 experiments were carried out in a wave basin at the University of Florida Coastal and Oceanographic Engineering Laboratory, in which wave run-up was measured for steep regular waves passing a fixed vertical cylinder with a radius, a, of 16.25 cm in a water depth, h_0, of 45 cm. The water depth ranged from nearly deep water with $\lambda/h_0 = 2.478$ to shallow water with $\lambda/h_0 = 8.378$. And k_0H values ranged from 0.085 to 0.806. Since the governing equations used in this paper is the Boussinesq equations which are based on the assumption of shallow water depth and the requirement that the nonlinearity $\varepsilon = k_0A$ be small, only cases 1–13 shall be examined as the water depth ranged from shallow water with $\lambda/h_0 = 8.378$ to near shallow water with $\lambda/h_0 = 6.065$ and the nonlinearity ε ranged from 0.0498 to 0.1940, see Table 1.

Table 1
Parameters in Kriebel's [33,34]

Cases	k_0	k_0a	k_0h_0	λ/h_0	μ^2	ε	k_0H
1	1.668	0.271	0.750	8.378	0.0143	0.0880	0.132
2						0.1187	0.178
3						0.1433	0.215
4	1.895	0.308	0.853	7.366	0.0184	0.0498	0.085
5						0.0803	0.137
6						0.1067	0.182
7						0.1465	0.250
8						0.1735	0.296
9	2.302	0.374	1.036	6.065	0.0272	0.0589	0.122
10						0.0989	0.205
11						0.1380	0.286
12						0.1858	0.385
13						0.1940	0.402

As the cylinder can be regarded as a special conical island, the toe Γ_0 of the cylinder and the coastline Γ_i are coincident. In our calculation, it is found that satisfactory results can be obtained by choosing the radius R of the artificial boundary $\mathscr{B}$ in the range $6.3a \leqslant R \leqslant 9a$. In this paper, the artificial boundary $\mathscr{B}$ is taken to be a circle of radius $R = 7.5a$. For all the 13 cases, 16 quadratic elements (with 32 boundary nodes) are used in each of the two boundary circles Γ_i and $\mathscr{B}$ and 72 internal collocation points are evenly distributed on six inner circles, the radius of which are $r_j = a + c_j(R - a)$ with c_j being 0.10, 0.26, 0.42, 0.58, 0.70 and 0.86 for $j = 1, \ldots, 6$, respectively. The results of the wave run-ups by experiments [34], the linear diffraction theory [1], Kriebel's second-order diffraction theory [33,34] and the present PDRBEM numerical model are presented in Figs. 2–8 (left), denoted by PDRBEM-B. In addition, for convenience of comparison, results of the present PDRBEM numerical model based on the Airy's equation are also displayed.

First of all, as expected, the first-order solutions, $\eta_0(x, y)$, of the PDRBEM for all 13 cases agree with the linear diffraction theoretical solutions [1] very well. For clarity, all these first-order solutions are not graphed in these figures.

Secondly, as shown in Figs. 2–8 (left), the maximum run-ups increased by taking nonlinearity into account, the more so the higher the incoming wave. The dispersive and nonlinear contribution from the PDRBEM model can indeed be significant. It can be seen that, at the front side ($\theta = 180^\circ$) of the cylinder, the linear diffraction theory badly underestimates the maximum wave run-ups in all cases with measured run-ups exceeding the linear theory by 13–78% and by 46% on average. In contrast, measured

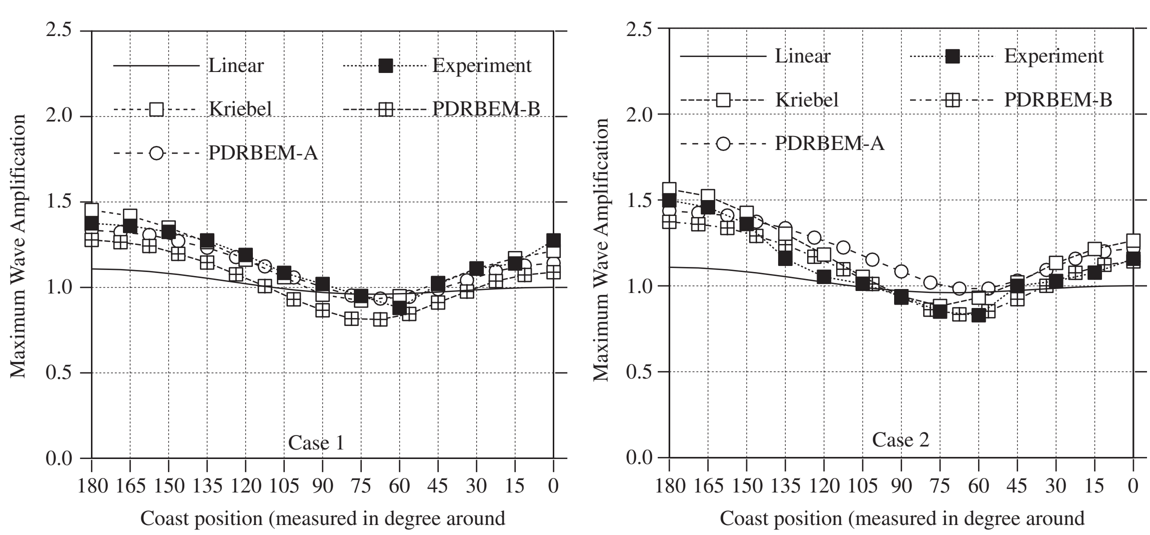

Fig. 2. Comparison among the experimental data [33,34], linear run-ups [1], the second order diffraction run-ups [33,34], the present weakly nonlinear run-ups based on the Boussinesq equations (PDRBEM-B) and the present weakly nonlinear run-ups based on the Airy equations (PDRBEM-A) for case 1 (left) and case 2 (right).

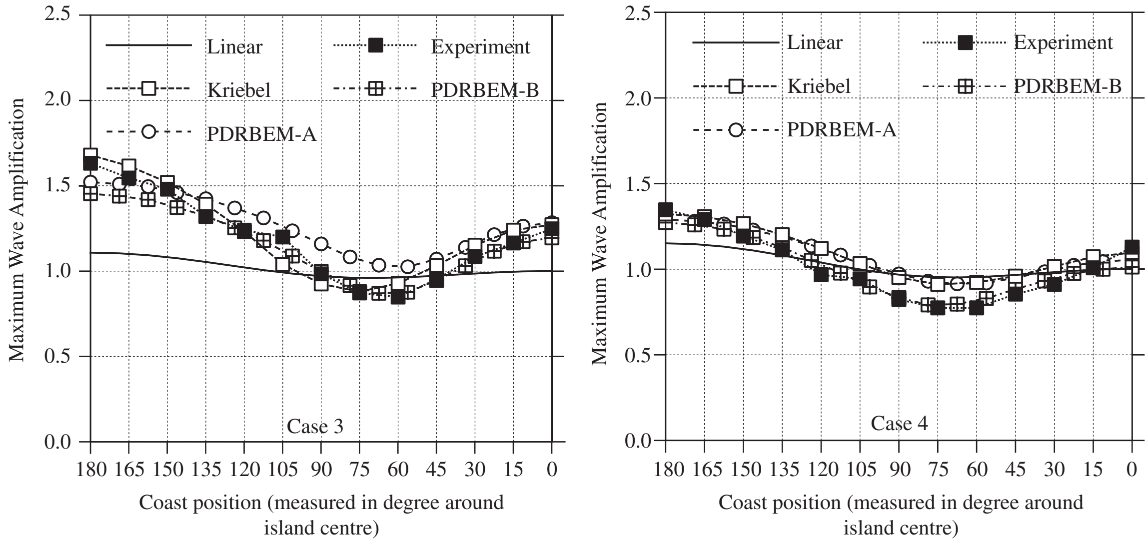

Fig. 3. Comparison among the experimental data [33,34], linear run-ups [1], the second order diffraction run-ups [33,34], the present weakly nonlinear run-ups based on the Boussinesq equations (PDRBEM-B) and the present weakly nonlinear run-ups based on the Airy equations (PDRBEM-A) for case 3 (left) and case 4 (right).

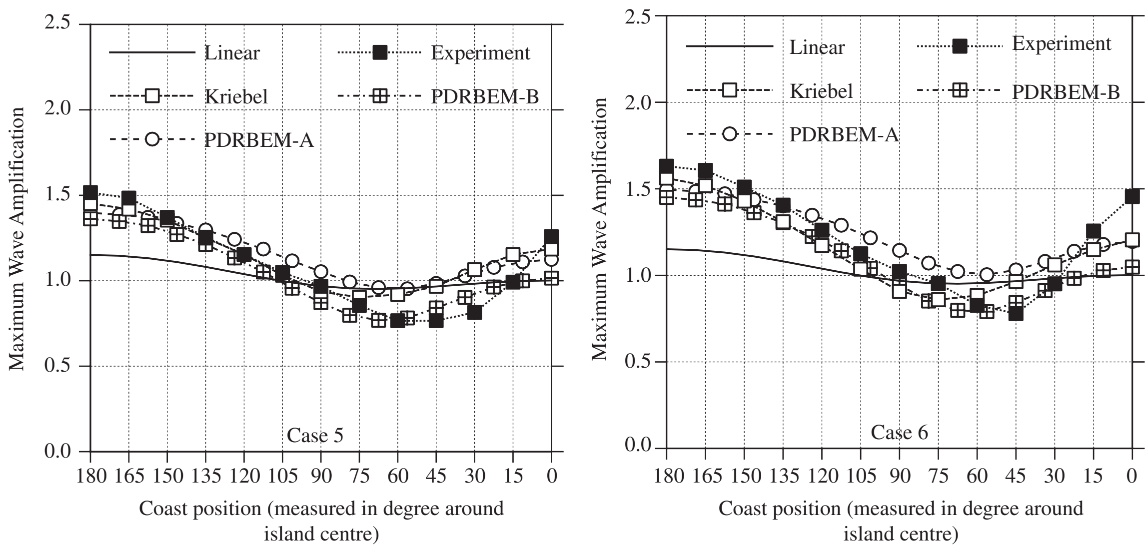

Fig. 4. Comparison among the experimental data [33,34], linear run-ups [1], the second order diffraction run-ups [33,34], the present weakly nonlinear run-ups based on the Boussinesq equations (PDRBEM-B) and the present weakly nonlinear run-ups based on the Airy equations (PDRBEM-A) for case 5 (left) and case 6 (right).

run-ups exceed the PDRBEM solution by up to 17% but by only 8% on average. Furthermore, the run-up distributions around the circumference are also poorly predicted by linear diffraction theory whereas the agreements between the measured run-ups and the PDRBEM run-ups are excellent in all 13 cases. Especially, for cases 2–5 and 9–13, the measured run-up profile is almost exactly replicated over all angular positions by the current PDRBEM model.

On the other hand, some differences between the present PDRBEM solutions and Kriebel's [33,34] second-order diffraction theory can be noticed. In fact, by comparing to the experiment data, it can be seen that Kriebel's second-order model performs better than the PDRBEM model in cases 1–3 and 6 but the latter performs better in cases 4 and 11–13. Theoretically, it is clear that the second order perturbation solution to a weakly dispersive approximation of the exact Laplace problem cannot produce a better result than a second order perturbation solution to the original fully dispersive problem. However, firstly, it is worth indicting that the perturbated expansion used in Kriebel's model is different from the expansion used in our model as there is an extra dispersive term proportional to μ^2 in our expansion (5). Strictly speaking, the perturbation expansion without the dispersive term based on the Airy equations is a two-dimensional version of Kriebel's three-dimensional perturbation expansion. This means that when the nonlinearity is small, the two-dimensional perturbation solution based on the Airy's theory should coincide with the three-dimensional Kriebel's solution. In fact, in cases 1, 4, 5 and 9, the nonlinear parameter ε is relatively small, being 0.0880, 0.0498, 0.0803 and 0.0589, respectively, the solution from Airy's theory does fit the Kriebel's theory very well. Secondly, the second-order far-field radiation condition used in the present PDRBEM is an approximation form of the Sommerfeld radiation condition, and the radiation condition used in Kriebel's second-order diffraction theory is a superposition of infinite

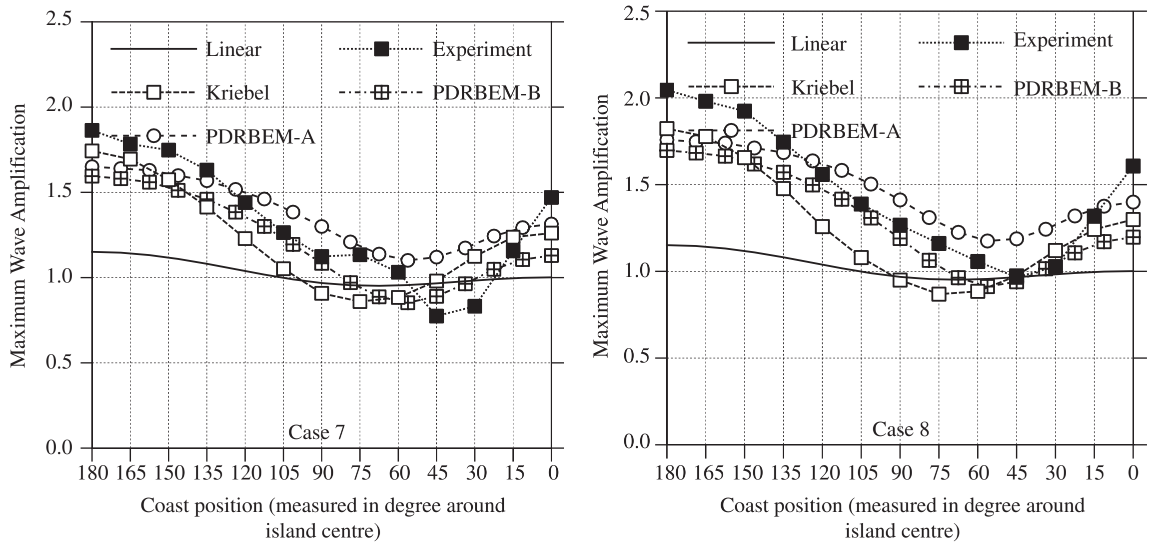

Fig. 5. Comparison among the experimental data [33,34], linear run-ups [1], the second order diffraction run-ups [33,34], the present weakly nonlinear run-ups based on the Boussinesq equations (PDRBEM-B) and the present weakly nonlinear run-ups based on the Airy equations (PDRBEM-A) for case 7 (left) and case 8 (right).

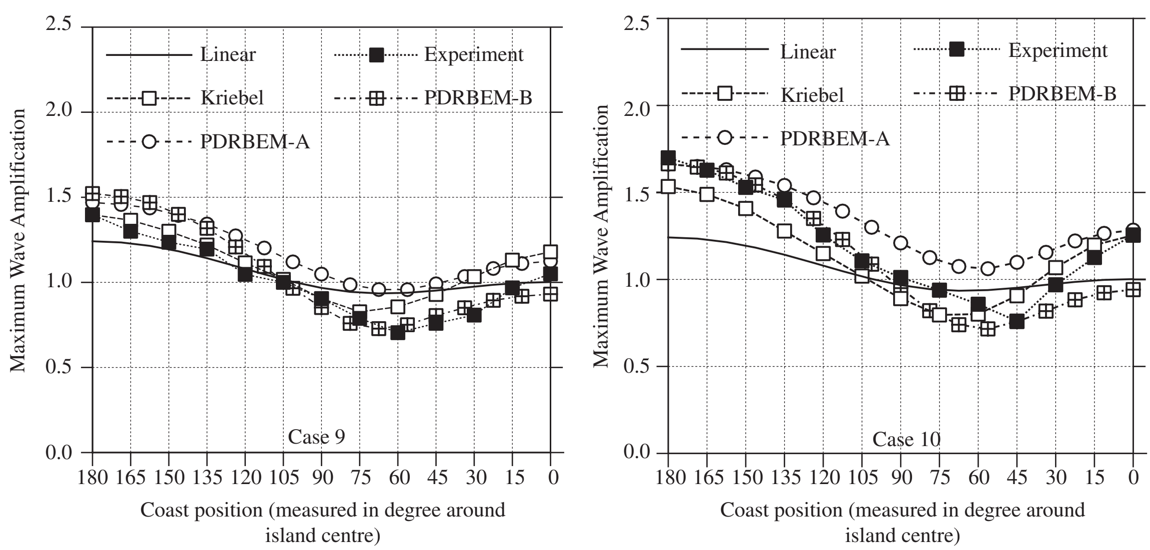

Fig. 6. Comparison among the experimental data [33,34], linear run-ups [1], the second order diffraction run-ups [33,34], the present weakly nonlinear run-ups based on the Boussinesq equations (PDRBEM-B) and the present weakly nonlinear run-ups based on the Airy equations (PDRBEM-A) for case 9 (left) and case 10 (right).

localized Sommerfeld radiation conditions with respect to infinite source points. Hence, it is no wonder there are some slight discrepancy between Kriebel's second-order diffraction theory and our PDRBEM model, after all, the agreement between two solutions is overall satisfactory.

In addition, as shown in Table 1, all 13 cases correspond to three different wavenumbers. The corresponding linear [1] and weakly nonlinear solutions of the wave run-ups for these four wavenumbers are separately graphed in Figs. 8 (right) and 9. In each group, although the amplitudes of all the cases are different, the linear solutions are the same since they correspond to the same wavenumber. However, as we can see from the weakly nonlinear solutions in all the three graphs, as the amplitude of the incident waves increases, the maximum wave run-up increases.

6.2. Combined refraction and diffraction on a conical island

We now apply the PDRBEM model to the combined wave refraction and diffraction on a conical island. Up to now, only a handful published experimental data on run-up of periodic waves around conical islands could be found in the literature. Among them are Lin and Hsiao [57], Hsiao et al. [58], Provis [59] and Liu et al. [7]. Both Lin and Hsiao [57] and Hsiao et al. [58] were focused on wave-current interaction and thus are not suitable for the current study. Provis' experiments were conducted in a small basin (5.55 m wide and 5.80 m long). The base diameter of the island was 3 m and the slope was 1:10. The water depth in the constant-depth region in the experiments was 0.15 m. Provis reported large discrepancies between his experimental data and theoretical results predicted by Smith and Sprinks [17]. Sprinks and Smith [60] pointed out later that because of the relatively small size of the wave basin and the shallow-water depth, the viscous damping and standing waves between the wave generator and the island contaminated the experimental results. In addition, in order to reduce the nonlinear effect, the wave amplitudes were kept as small as possible, the incident wave typically having a amplitude of 0.00005 m. Provis' experiments are inappropriate for testing our PDRBEM model.

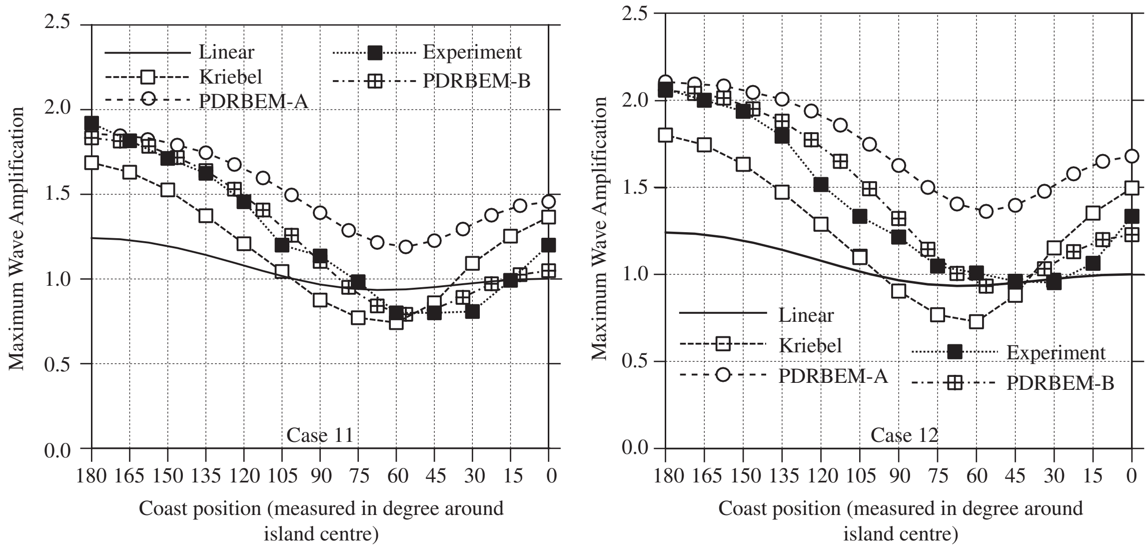

Fig. 7. Comparison among the experimental data [33,34], linear run-ups [1], the second order diffraction run-ups [33,34], the present weakly nonlinear run-ups based on the Boussinesq equations (PDRBEM-B) and the present weakly nonlinear run-ups based on the Airy equations (PDRBEM-A) for case 11 (left) and for case 12 (right).

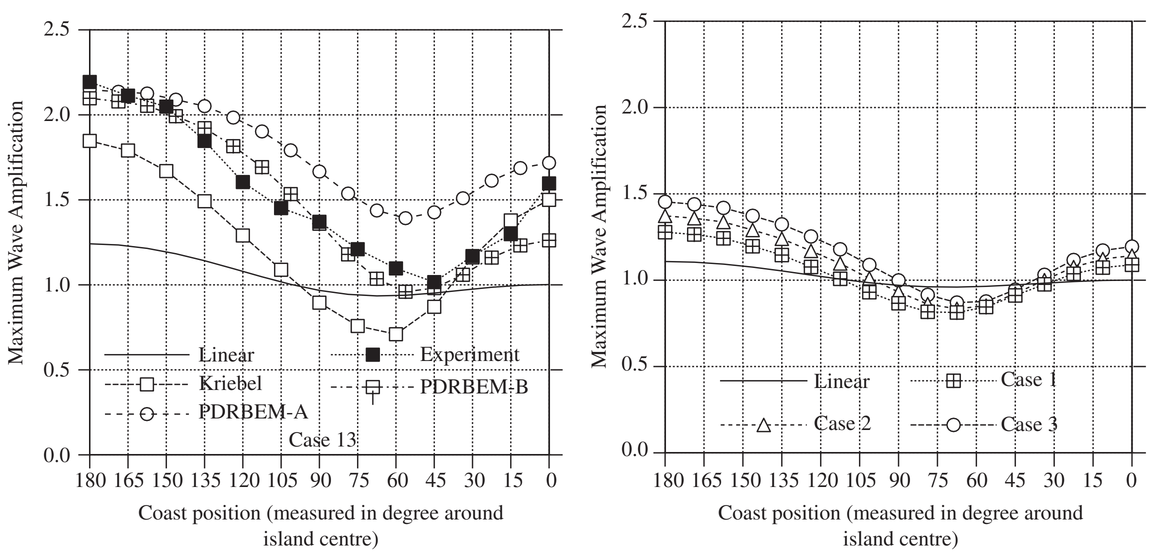

Fig. 8. Comparison among the experimental data [33,34], linear run-ups [1], the second order diffraction run-ups [33,34], the present weakly nonlinear run-ups based on the Boussinesq equations (PDRBEM-B) and the present weakly nonlinear run-ups based on the Airy equations (PDRBEM-A) for case 13 (left); Comparison between the linear diffraction run-ups and the present weakly nonlinear run-ups for cases 1–3 (right).

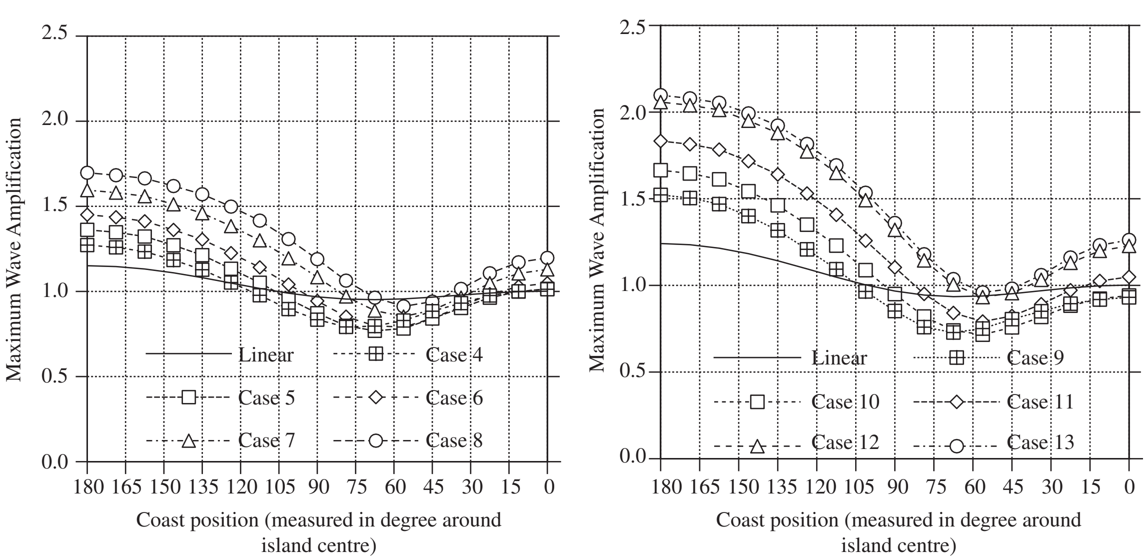

Fig. 9. Comparison between the linear diffraction run-ups and the present weakly nonlinear run-ups for cases 4–8 (left) and cases 9–13 (right).

We chose the experiments reported by Liu et al. [7] as numerical examples to test our PDRBEM model. The experiments were performed at the National Defence Academy (NDA), Japan. They were carried out in a small basin with 7 m width and 11 m length. The base diameter of the island was 3.3 m and the slope was 1:4. The water depth in the constant-depth region in the experiments was 0.1930–0.2955 m. These conditions together with the parameters of the incident waves are tabulated in Table 2.

Table 2
The parameters in the experiments used by Liu et al. [7]

Cases	a (m)	b (m)	h_0 (m)	A (m)	T (s)	ε	μ^2
1	0.468	1.65	0.2955	0.00250	4.5	0.00846	0.00149
2	0.468	1.65	0.2955	0.00085	2.5	0.00288	0.00483
3	0.878	1.65	0.1930	0.00285	3.0	0.01477	0.00219
4	0.862	1.65	0.1970	0.00235	2.5	0.01193	0.00322

In our numerical computation, for all these four cases the artificial boundary $\mathscr{B}$ is taken to be the toe, Γ_0, of the island. In addition, 20 quadratic elements (with 40 boundary nodes) are used in each of the two boundary circles Γ_i and Γ_0 and 72 internal collocation points are evenly distributed on six inner circles where their radius are $r_j = a + c_j(b-a)$ with c_j being 0.10, 0.26, 0.42, 0.58, 0.70 and 0.86 for $j = 1, \ldots, 6$, respectively.

In Fig. 10, the maximum run-ups are shown for experimental data, linear theory [3] based on the linear shallow-water equation, the time-marching finite difference scheme for the nonlinear shallow-water equations [7] and the present PDRBEM based on the Boussinesq equations. As we can see from Table 2, the nonlinearity is weakest in cases 1 and 2 while the dispersive effects are weakest in cases 1 and 3. For cases 1 and 3 all the different theories lie close together. For case 1 there is an excellent comparison with experimental results while for case 3 there is

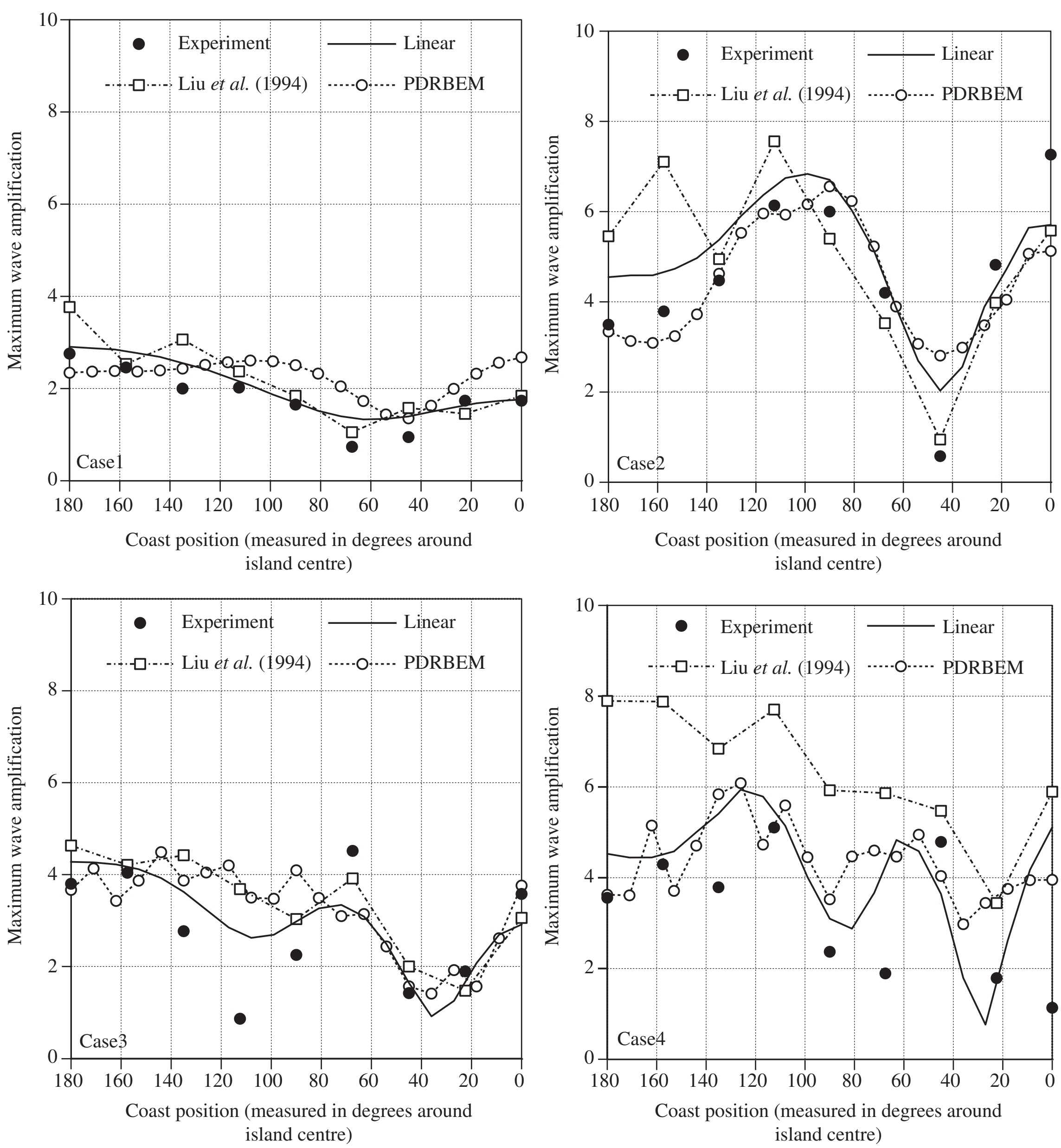

Fig. 10. Comparison among the experimental data, the linear analytical run-ups [3], the nonlinear shallow-water run-ups [7] and the PDRBEM run-ups.

some variation between the experimental results and theory near the 120° region.

In cases 2 and 4, for which dispersion is important, Liu et al. [7] results diverge significantly from the other results. This is due to the fact no-dispersive terms are present in the nonlinear shallow-water equations. The present PDRBEM method does extremely well in case 2 while there is some divergence between all the theories and the experimental results near $\theta = 0^\circ$ for case 4.

Significant unexplained differences between the PDRBEM solutions and experimental data are observed in both cases 3 and 4. These are the cases in which the nonlinear effects are largest so perhaps neglected higher-order nonlinear terms are the cause of these variations.

7. Conclusions

In this paper, a weakly nonlinear numerical model, called the PDRBEM model, is presented for wave diffraction and refraction governed by the Boussinesq equations. To validate this new model, wave diffraction by a vertical cylinder has been first calculated and the maximum wave run-ups around the cylinder have been compared with experimental results, linear solutions and the second order diffraction solutions. It is shown that, for water depth ranging from shallow water to near-deep water, the dispersive and nonlinear effects of the new model are significant and our model is very accurate. Then, the model is applied to the combined wave diffraction and refraction by a conical island. The nonlinear and linear wave run-ups around the conical island are calculated and commented upon.

Our new model is very useful for a number of reasons. Firstly it is much more accurate than linear models as weakly nonlinear effect and dispersion have been included. Moreover, since frequency decomposition has been used and the time-dependent governing equations have been transformed into three time-independent linear equations, our model does not require time-marching. Also, the domain integrals have been transformed into evaluation on some distributing collocation points over the domain. Hence our model is much more computationally efficient than other numerical schemes which include nonlinear effects.

Acknowledgements

We would like to thank an anonymous referee, who has provided many useful suggestions and references for us to improve the presentation of this paper. The second author would also like to thank the financial support from a Australian Government Overseas Postgraduate Research Scholarship and from a University of Wollongong Postgraduate Award. He is also gratefully acknowledge the financial support from the Natural Science Foundation of China (10462001), the Funding for Returning Overseas Scholars of China State Education Ministry (2005-35), Guangxi Natural Science Foundation (0575029, 0639008) and Guangxi Shi-Bai-Qian Scholars Program (2001224).

References

[1] MacCamy RC, Fuchs RA. Wave forces on piles: a diffraction theory. US Army Corps of Engineering, Beach Erosion Board, Washington, DC, Technical Mem 69, 1954.
[2] Homma S. On the behaviour of seismic sea waves around circular island. Geophys Mag 1950;21:199–208.
[3] Zhang YL, Zhu S-P. New solutions for the propagation of long water waves over variable depth. J Fluid Mech 1994;278:391–406.
[4] Zhu S-P, Zhang YL. Scattering of long waves around a circular Island mounted on a conical shoal. Wave Motion 1995;23:353–62.
[5] Liu H-W, Lin P-Z, Shankar NJ. An analytical solution of the mild-slope equation for waves around a circular island on a paraboloidal shoal. Coastal Eng 2004;51(5–6):421–37.
[6] Lautenbacher CC. Gravity wave refraction by islands. J Fluid Mech 1970; 41:655–72.
[7] Liu PL-F, Cho Y-S, Fujima KJ. Numerical solutions of three-dimensional run-up on a circular island. In: International symposium: waves-physical and numerical modelling, University of British Columbia, Vancouver, Canada, 1994. p. 1031–40.
[8] Liu PL-F, Cho Y-S, Briggs MJ, Kanoglu U, Synolakis CE. Runup of solitary waves on a circular island. J Fluid Mech 1995;302:259–85.
[9] Chen HS, Mei CC. Oscillations and wave forces in a Man-made Harbor in the open sea. TR no. 190, Ralph M. Parsons Laboratory, Department of Civil Engineering, MIT, 1974.
[10] Bettess P, Zienkiewicz OC. Diffraction and refraction of surface waves using finite and infinite elements. Int J Numer Methods Eng 1977;2:1271.
[11] Houston JR. Combined refraction and diffraction of short waves using the finite element method. Appl Ocean Res 1981;3:163.
[12] Jonsson IG, Skovgaard O, Brink-Kjaer O. Diffraction and refraction calculations for waves incident on an island. J Mar Res 1976;34:469–96.
[13] Au MC, Brebbia CA. Diffraction of water waves for vertical cylinders using boundary elements. Appl Math Modelling 1983;7:106–14.
[14] Zhu S-P. A new DRBEM model for wave refraction and diffraction. Eng Anal Boundary Elements 1993;12:261–74.
[15] Zhu S-P, Liu H-W, Chen K. A general DRBEM model for wave refraction and diffraction. Eng Anal Boundary Elements 2000;24:377–90.
[16] Liu H-W. Numerical modelling of the propagation of ocean waves. Doctoral dissertation. University of Wollongong, Wollongong, Australia, 2001.
[17] Smith R, Sprinks T. Scattering of surface waves by a conical island. J Fluid Mech 1975;72:373.
[18] Kanoglu U, Synolakis CE. Long wave runup on piecewise linear topographies. J Fluid Mech 1998;374:1–28.
[19] Peregrine DH. Long waves on a beach. J Fluid Mech 1967;27:815–27.
[20] Abbott MB, Petersen HM, Skovgaard O. On the numerical modelling of short waves in shallow water. J Hydraulic Res 1978;16:173–204.
[21] Rygg O. Nonlinear refraction–diffraction of surface waves in intermediate and shallow water. Coastal Eng 1988;12:191–211.
[22] Nwogu O. An alternative form of the Boussinesq equation for nearshore wave propagation. J Waterway Port Coastal Ocean Eng 1993;119:618–38.
[23] Wei G, Kirby JT. Time-dependent numerical code for extended Boussinesq equations. J Waterway Port Coastal Ocean Eng 1995;121:251–61.
[24] Wei G, Kirby JT, Grilli ST, Subramanya R. A fully nonlinear Boussinesq model for surface waves, part 1: highly nonlinear unsteady waves. J Fluid Mech 1995;294:71–92.
[25] Chen Q, Kirby JT, Dalrymple RA, Kennedy AB, Chawla A. Boussinesq modeling of wave transformation, breaking and runup. J Waterway Port Coastal Ocean Eng 2000;126:48–56.
[26] Liu PL-F, Yoon SB, Kirby JT. Nonlinear refraction–diffraction of waves in shallow water. J Fluid Mech 1985;153:185–201.
[27] Chen Y, Liu PL-F. Modified Boussinesq equations and associated parabolic model for water wave propagation. J Fluid Mech 1995;288:351–81.
[28] Hwang L-S, Tuck EO. On the oscillations of harbours of arbitrary shape. J Fluid Mech 1970;42:447–64.
[29] Nardini D, Brebbia CA. A new approach to free vibration analysis using boundary elements. In: Brebbia CA, editor. Boundary element methods in engineering. Berlin: Springer; 1982.
[30] Hsiao SS, Wu JH, Chiu YF. A perturbation-DRBEM model for wave refraction–diffraction. In: Seventh international offshore and polar engineering conference (ISOPE-97), Honolulu, USA, 1997. p. 308–12.
[31] Hsiao SS, Weng WK, Chiu YF. Wave force on a circular island using perturbation-DRBEM. In: The eighth international offshore and polar engineering conference (ISOPE-98), vol. 1, Montreal, Canada, 1998. p. 231–6.
[32] Rangogni R. A simple procedure to solve the mild-slope equation using BEM and perturbation expansion technique—part 1. In: Brebbia CA, editor. Boundary elements X, vol. 1. Southampton, Berlin: Computational Mechanics Publications, Springer; 1988. p. 331–43.
[33] Kriebel DL. Nonlinear wave interaction with a vertical circular cylinder part, I: diffraction theory. Ocean Eng 1990;17:345–77.
[34] Kriebel DL. Nonlinear wave interaction with a vertical circular cylinder, part II: wave runup. Ocean Eng 1992;19:75–99.
[35] Mei CC. The applied dynamics of ocean surface waves. Singapore: World Scientific; 1989.
[36] Sommerfeld A. Partial differential equations in physics. New York: Academic Press; 1949.
[37] Givoli D. Non-reflecting boundary conditions. J Comput Phys 1991;94: 1–29.
[38] Engquist E, Majda A. Absorbing boundary conditions for the numerical simulation of waves. Math Comput 1977;31:629–51.
[39] Molin B. Second order diffraction loads upon three-dimensional bodies. Appl Ocean Res 1979;1:197–202.
[40] Newman JN. The second-order wave force on a vertical cylinder. J Fluid Mech 1996;320:417–43.
[41] Nardini D, Brebbia CA. Transient boundary element elastidynamics using the dual reciprocity method and model superposition. In: Boundary element VIII, vol. 1. Southampton, Berlin: Computational Mechanics Publications, Springer; 1986.

[42] Partridge PW, Wrobel LC. The dual reciprocity method for spontaneous ignition. Int J Numer Methods Eng 1990;30:953–63.
[43] Zhu S-P, Zhang YL. Improvement on dual reciprocity boundary element method for equations with convective terms. Commun Numer Methods Eng 1994;10:361–71.
[44] Zhang YL, Zhu S-P. On the choice of interpolation functions used in the dual-reciprocity boundary-element method. Eng Anal Boundary Elements 1994;13:387–96.
[45] Partridge PW, Brebbia CA. Computer implementation of the BEM dual reciprocity method for the solution of Poisson type equations. Software Eng Workstations 1989;5:199–206.
[46] Lu X-P. On the application of the thin plate spline in the LTDRM for solving linear and nonlinear diffusion problems. In: Proceedings of the second biennial Australian engineering mathematics conference, Sydney, Australia, 1996. p. 437–43.
[47] Zhu S-P, Liu H-W, Lu X-P. A combination of the LTDRM and the ATPS in solving diffusion problems. Eng Anal Boundary Elements 1998;21(3):285–9.
[48] Zhu S-P, Liu H-W. On the application of the generalized multiquadric bases in conjunction with the LTDRM to solve transient nonlinear diffusion equations. Appl Math Comput 1998;96:161–75.
[49] Chen JT, Chang MH, Chen KH, Lin SR. The boundary collocation method with meshless concept for acoustic eigenanalysis of two-dimensional cavities using radial basis function. J Sound Vib 2002;257(4):667–711.
[50] Chen JT, Chen IL, Chen KH, Yeh YT, Lee YT. A meshless method for free vibration of arbitrarily shaped plates with clamped boundaries using radial basis function. Eng Anal Boundary Elements 2004;28(5):535–45.
[51] Reutskiy SY, Chen CS. Approximation of multivariate functions and evaluation of particular solutions using Chebyshev polynomial and trigonometric basis functions. Int J Numer Methods Eng 2006;67:1811–29.
[52] Hsiao S-S, Chang J-R, Chang C-M. Improving the accuracy of DRBEM wave model by using radial basis function. In: Proceedings of the seventeenth international offshore and polar engineering conference, Lisbon, Portugal, 2007. p. 2296–301.
[53] Micchelli CA. Interpolation of scattered data: distance matrices and conditionally positive definite functions. Constr Approx 1986;2:11–22.
[54] Zhu S-P. Particular solutions associated with the Helmholtz operator used in DRBEM. Boundary Elements Abstr 1993;4:231–3.
[55] Fairweather G, Karageorghis A. The method of fundamental solutions for elliptic boundary value problems. Adv Comput Math 1998;9:69–95.
[56] Li J, Hon YC, Chen C-S. Numerical comparisons of two meshless methods using radial basis functions. Eng Anal Boundary Elements 2002;26(3): 205–25.
[57] Lin MC, Hsiao SS. Experimental study on wave-current interactions around a large scale cylinder. Coastal Eng Jpn 1995;38(1):39–61.
[58] Hsiao SS, Weng WK, Lin MC. Wave pressure on a large cylinder in a wave-current coexisting field. In: The ninth international offshore and polar engineering conference, Brest, France, 1999. p. 441–5.
[59] Provis DG. Propagation of water waves near an island. PhD thesis, University of Essex, 1975.
[60] Sprinks T, Smith R. Scale effects in a wave-refraction experiment. J Fluid Mech 1983;129:455–71.